Springer

KSME

Journal of Mechanical Science and Technology 31 (7) (2017) 3519~3529
www.springerlink.com/content/1738-494x(Print)/1976-3824(Online)
DOI 10.1007/s12206-017-0640-0

Research on PSA-MFAC for a novel bionic elbow joint system actuated by pneumatic artificial muscles †

Hui Yang, Chaoqun Xiang, Lina Hao*, Liangliang Zhao and Bangcan Xue

School of Mechanical Engineering & Automation, Northeastern University, Shenyang, 110819, China

(Manuscript Received April 13, 2016; Revised March 11, 2017; Accepted March 20, 2017)

Abstract

A 3-DOF bionic elbow joint actuated by Pneumatic artificial muscle (PAM) was designed in this paper, and its inverse kinematics model was also established. Then, based on the Model-free adaptive control (MFAC) theory and the effects of control parameters to the control system, a Parameter self-adjust Model-free adaptive control (PSA-MFAC) strategy was proposed, and its adaptability for different control objects was also tested in simulation environment. Combined with the inverse kinematics model, motion control experiments of the bionic elbow joint were conducted in semi-physical platform. Compared with conventional MFAC and PID control algorithm, the experiment results strongly verified the improvement of PSA-MFAC control accuracy. The tracking accuracy of conventional MFAC and PID controller were 9.5 % and 15 %, respectively, in contrast, the PSA-MFAC controller was only 3.8 %. Moreover, complex dynamics modelling of the elbow joint and adjusting process of control parameters were neglected in PSA-MFAC control system.

Keywords: PAM; Bionic elbow joint; Inverse kinematics model; PSA-MFAC

1. Introduction

Pneumatic artificial muscle (PAM) is a novel compliance actuator, which can be categorized into netted muscles, embedded muscles and braided muscles. The McKibben muscle belongs to braided muscles invented by Joseph L. McKibben and widely applied in engineering. This kind of PAM is composed of an elastomeric bladder, a braided mesh sleeve and two connecting attachments. By inflation of the elastomeric bladder, the braided mesh sleeve and the bladder expand in radial direction and contract in axial direction. Meanwhile, a contraction force is generated in axial direction [1, 2].

The PAM has lots of potential advantages, especially, the high power density, good safety and compliance property. Due to the power density of PAM can reach 10 Kw/Kg and the actuating propriety of PAM is the same as human muscles, it is widely used in the fields of rehabilitation therapy and bionic actuating [3-7]. However, PAM has some inherent drawbacks such as the friction and nonlinear deformation, which makes the dynamic modeling and motion controlling very difficult and restricts the PAM application. Due to the above mentioned problems, currently researches focus on model-based control methods and model-free control methods. The achievements of model-based control are relying on means of accurate dynamical model of PAM, which has considered friction, hysteresis and other nonlinear factors, combined with intelligent control algorithm on precise motion control of PAM actuator. Typical works have been conducted such as, George et al. at University of Patras established statics and dynamics models of PAM [8], then switch piecewise affine system approximate model was obtained, Switch model predictive control (SMPC) method could be employed based on it. Then, optimum control and the control effort's smooth transition for PAM actuator were achieved. Jouppila at University of Tampere built a dynamic model, a pressure model of PAM [9], and a fluid mass of high speed switch valve model, then a sliding mode control method was applied to the PAM actuating system. The entire integrated system had a good robustness in variation of load situation. Ryan at University of Maryland did some researches on heavy duty crane mechanical arm actuated by PAM [10]. Based on flow dynamics, structure parameters of PAM and dynamical model of the manipulator, the feed-forward PID controller and the fuzzy controller had been designed and compared in the system. Kang at Hannam University analyzed the compliance propriety of an antagonism PAM manipulator [11], and proposed a sliding mode force control strategy based on the variable rigidity propriety of PAM. The control precision of the control scheme was greatly improved, which was compared with that of the conventional PID control. Zhu at Zhejiang University took parallel manipulator actuated by PAMs as research object

*Corresponding author. Tel.: +86 13390158387, Fax.: +86 13390158387
E-mail address: haolina@me.neu.edu.cn
† Recommended by Associate Editor Sangyoon Lee

[12]. Considering time-dependent friction, static force modeling errors, and strong coupling nonlinear characteristics, an adaptive robust control strategy was proposed, which made PAM actuated mechanical arm have a desired tracking accuracy. However, model-based control methods have a strong dependence on dynamic model precision of PAM. Moreover, complex control laws, a large number of control parameters and sophisticated process of system parameters make the methods hard to realize in control systems [13, 14]. To fulfill the aim of reliable and practical controller design for complex systems, some researchers have been focusing on the so-called model-free control strategies.

Tondu at University of Toulouse proposed a method that the natural stiffness and damping of PAM were substituted by a conventional PID controller which only has one control parameter (Ki). Then, the complex dynamical model was neglected [15]. An evolutional fuzzy PID controller was proposed by Chang at Louis university of Wisconsin [16]. The recurrent neuro-fuzzy model of the PAM was set up based on experimental data, replacing of dynamic model of PAM, and the control effect was satisfactory for the system. Anh at University of Ulsan applied modified genetic algorithm to establish and identify the nonlinear auto-regression fuzzy inverse model, and then designed the NARX fuzzy PID controller [17]. This controller worked well to solve the nonlinear property of PAM.

Model-free adaptive control (MFAC) method was first proposed by Hou at Beijing Jiaotong University in 1994. This control strategy adopts an innovative dynamic linearization method and introduces Pseudo partial derivative (PPD) concept for the discrete-time nonlinear system. An equivalent dynamic linear data model should be established at each dynamic working point in the closed-loop system, and then the system controller was designed based on the above data model. Therefore, the self-adaptive control can guarantee a good performance for a nonlinear system [18, 19]. In terms of the PAM control, only Liu at Beijing Institute of Technology introduced the algorithm in application of a globe joint robot. Although the control effect was reported well, the control parameters adjustment was complex [20].

In this paper, a novel PAM bionic elbow joint is designed and its inverse kinematics model is established. Then, a Parameters self-adjust Model-free adaptive control (PSA-MFAC) strategy are proposed by considering the control parameters characteristics of MFAC and using the gradient descent method. This control scheme is independent of complex dynamic model, and shows the favourable control accuracy. Moreover, the adjustment process of control parameters for different control objects is also avoided, which means the control strategy has good adaptability. Combined with the inverse kinematics model, the PSA-MFAC is tested on the bionic elbow joint and shows better dynamic performances than PID and conventional MFAC algorithm.

The rest parts of the article are presented as follows. In Sec. 2, a novel PAM bionic elbow joint is designed and its inverse kinematic model is established. In Sec. 3, the PSA-MFAC scheme is presented and its adaptability is simulated and analyzed. According to the inverse kinematic model of the elbow joint, Sec. 4 gives PID, MFAC and PSA-MFAC control schemes for trajectory tracking tests of the experimental measurement system. Meanwhile, the experimental test is conducted and results are analyzed. Finally, conclusions are given in Sec. 5.

Table 1. Upper arm parameters.

Upper arm length (mm)	Sagittal diameter of humeral head (mm)	Movement range of elbow joint (°)
313	40.1±3.9	-5~142

Table 2. Design parameters of PAM bionic elbow joint.

Elbow joint length	Elbow joint width	Flexion and extension of elbow joint	Adduction and abduction of elbow joint	Internal and external rotation of elbow joint
297 mm	38 mm	0°~100°	0°~100°	0°~20°

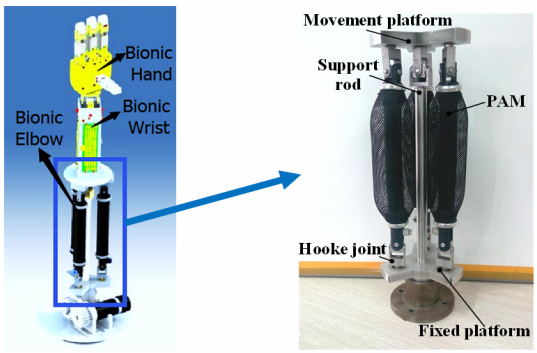

Fig. 1. PAM bionic elbow joint.

2. Structure design and inverse kinematics modeling

2.1 Structure design of PAM bionic elbow joint

Based on the upper arm parameters of Chinese adult men shown in Table 1 (Chinese standards: GB10000-88 and GB/T13547-92), the key design parameters of the PAM bionic elbow joint are presented in Table 2.

Due to the advantages of the parallel mechanism such as its structure is simple, and it has no accumulative error and a high carrying capacity, the bionic elbow joint is designed based on the 3-connecting rods parallel mechanism which has a simple kinematics model and a dynamics model. According to design parameters, three Shadow 30 mm air muscles are used as actuators for bionic elbow joint, as shown in Fig. 1. For the Shadow 30 mm air muscle, the minimum muscle length, the maximum muscle length and the initial muscle length are 150 mm, 230 mm and 180 mm, respectively.

From Fig. 1, the bionic elbow joint as one part of a humanoid manipulator mainly consists of a fixed platform, a movement platform, a support rod, three PAMs and seven Hooke

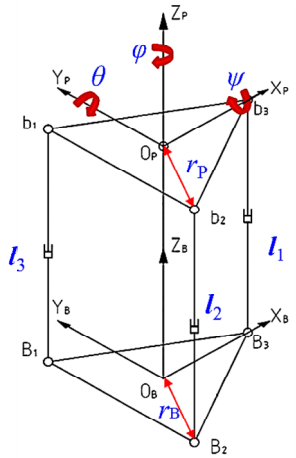

Fig. 2. Spatial coordinate systems of bionic elbow joint.

joints. Four Hooke joints are mounted on the fixed platform and the others are attached to the movement platform. The air inlet end of the PAM is connected with the fixed platform and the other end is connected with the movement platform through two Hooke joints, respectively. The means of the connection between the upper end of the support rod and the movement platform is by a Hooke joint, and the lower end is fixedly connected to the fixed platform via a screw thread. The lengths could be changed by adjusting the inflation pressures of the three PAMs independently, which results in the movement platform rotation about three axes.

2.2 Inverse kinematics modeling of PAM bionic elbow joint

For the PAM bionic elbow joint, the three PAMs lengths and the movement platform rotation angles are input variables and output variables, respectively. To control the movement platform rotation angles, the lengths of PAMs should be controlled and it is necessary to build the inverse kinematics model of the PAM bionic elbow joint.

Set spatial coordinate systems as shown in Fig. 2.

As showed in Fig. 2, a fixed coordinate system O_B-$X_BY_BZ_B$ and a moving coordinate system O_p-$X_pY_pZ_p$ are established, respectively, at the center of the fixed platform and at the center of the movement platform. The fixed coordinate system O_B-X_B Y_B Z_B as a reference system, and the rotation matrix R of the coordinate system O_p-$X_pY_pZ_p$ relative to it is given by Eq. (1):

$$\begin{aligned}\mathbf{R} &= \mathbf{R}_X(\psi)\mathbf{R}_Y(\theta)\mathbf{R}_Z(\phi)\\ &= \begin{pmatrix} \cos\phi\cos\theta & \cos\phi\sin\theta\sin\psi-\sin\phi\cos\psi & \cos\phi\sin\theta\cos\psi+\sin\psi\sin\phi \\ \sin\phi\cos\theta & \sin\phi\sin\theta\sin\psi+\cos\phi\cos\psi & \sin\phi\sin\theta\cos\psi-\sin\psi\cos\phi \\ -\sin\theta & \cos\theta\sin\psi & \cos\theta\cos\psi \end{pmatrix}\\ &= \begin{pmatrix} x_l & x_m & x_n \\ y_l & y_m & y_n \\ z_l & z_m & z_n \end{pmatrix}\end{aligned} \tag{1}$$

where ψ, θ and φ are the Euler angles about all three axes (X_B, Y_B, Z_B), and the clockwise direction about each axis is positive.

According to the position coordinate of the moving coordinate system origin $\boldsymbol{P}=(0, 0, h)^T$, expressed in the fixed coordinate system , the length l_i (i = 1, 2, 3) of each PAMs as follows:

$$l_i^2 = (\mathbf{P}+\mathbf{R}\mathbf{b}_i-\mathbf{B}_i)(\mathbf{P}+\mathbf{R}\mathbf{b}_i-\mathbf{B}) \qquad (i=1,2,3) \tag{2}$$

where $\boldsymbol{b}_i = (b_{ix}, b_{iy}, b_{iz})^T$ is the position coordinate of the i^{th} Hooke joint on the movement platform in the moving coordinate system; $\boldsymbol{B}_i = (B_{ix}, B_{iy}, B_{iz})^T$ is the position coordinate of the i^{th} Hooke joint on the fixed platform in the fixed coordinate system; h is the height of the bionic elbow joint. After operation of the Eq. (2), the following relationship can be founded:

$$\begin{aligned} l_i^2 &= B_{ix}^2+B_{iy}^2+b_{ix}^2(x_l^2+y_l^2+z_l^2)+b_{iy}^2(x_m^2+y_m^2+z_m^2)\\ &\quad +2b_{ix}b_{iy}(x_lx_m+y_ly_m+z_lz_m)-2B_{ix}(b_{ix}x_l+b_{iy}x_m) \qquad (i=1,2,3)\\ &\quad -2B_{iy}(b_{ix}y_l+b_{iy}y_m)+2b_{ix}hz_l+2b_{iy}hz_m+h^2 . \end{aligned} \tag{3}$$

Based on the orthogonality of the rotation matrix $\boldsymbol{R}$, Eq. (3) can be written as:

$$\begin{aligned} l_i^2 &= B_{ix}^2+B_{iy}^2+b_{ix}^2+b_{iy}^2-2B_{ix}(b_{ix}x_l+b_{iy}x_m)-2B_{iy}(b_{ix}y_l+b_{iy}y_m)\\ &\quad +2b_{ix}hz_l+2b_{iy}hz_m+h^2 \qquad (i=1,2,3) . \end{aligned} \tag{4}$$

For the PAM bionic elbow joint, the movement platform radius r_P and the fixed platform radius r_B are equal, namely r_P = r_B = r. The coordinates of the Hooke joints $\boldsymbol{B}_i$ and $\boldsymbol{b}_i$, expressed in the fixed coordinate system and the moving coordinate system, respectively, are determined as follows:

$$\mathbf{b}_1=\begin{pmatrix} r \\ 0 \\ 0 \end{pmatrix}, \quad \mathbf{b}_2=\begin{pmatrix} -\frac{r}{2} \\ -\frac{\sqrt{3}}{2}r \\ 0 \end{pmatrix}, \quad \mathbf{b}_3=\begin{pmatrix} -\frac{r}{2} \\ \frac{\sqrt{3}}{2}r \\ 0 \end{pmatrix} \tag{5}$$

$$\mathbf{B}_1=\begin{pmatrix} r \\ 0 \\ 0 \end{pmatrix}, \quad \mathbf{B}_2=\begin{pmatrix} -\frac{r}{2} \\ -\frac{\sqrt{3}}{2}r \\ 0 \end{pmatrix}, \quad \mathbf{B}_3=\begin{pmatrix} -\frac{r}{2} \\ \frac{\sqrt{3}}{2}r \\ 0 \end{pmatrix} . \tag{6}$$

According to Eqs. (4)-(6), the length of each PAMs can be derived as follows:

$$\begin{cases} l_1=\sqrt{2r^2(1-x_l)+h(h+2rz_l)}\,; \\ l_2=\sqrt{2r^2+h^2-\frac{r^2}{2}(x_l+\sqrt{3}x_m+\sqrt{3}y_l+3y_m+\frac{2\sqrt{3}}{r}hz_m+\frac{2}{r}hz_l)}\,; \\ l_3=\sqrt{2r^2+h^2-\frac{r^2}{2}(x_l-\sqrt{3}x_m-\sqrt{3}y_l+3y_m-\frac{2\sqrt{3}}{r}hz_m+\frac{2}{r}hz_l)} . \end{cases} \tag{7}$$

Eq. (7) is the inverse kinematics model of the PAM bionic elbow joint, and it is necessary for the motion control of the bionic elbow joint.

3. PSA-MFAC controller design

3.1 MFAC introduction

Compared with conventional adaptive controllers, MFAC needn't any external test signals or training processes which are necessary for the nonlinear controllers based on neural network. In addition, for the closed-loop system, it ensures the monotonic convergence of tracking error and the stability of Bounded-input bounded-output (BIBO). Thus, the controller has been applied to the chemical process, the injection molding process, and so on [22-24]. The brief introduction of the control theory is as follows:

In Ref. [18], the discrete-time SISO nonlinear system is considered as follows:

$$y(k+1) = f(y(k),\cdots,y(k-j),u(k),\cdots,u(k-i)) \tag{8}$$

where i and j are orders of output $y(k)$ and input $u(k)$, respectively. $f(\ldots)$ is a smooth unknown nonlinear function.

The MFAC scheme is based on the following assumptions:

A1: The partial derivative of $f(.)$ about the system current input signal $u(k)$ is existence and continuity.

A2: The system Eq. (8) is generalized Lipschitz, for any $k_1 \neq k_2$, k_1, $k_2 \geq 0$ and $u(k_1) \neq u(k_2)$, there exists a parameter $b \in R$ makes the Eq. (9) be established.

$$\left|y(k_1+1) - y(k_2+1)\right| \leq b\left|u(k_1) - u(k_2)\right|. \tag{9}$$

Based on the assumptions A1 and A2, when $|u(k) - u(k\text{-}1)| \neq 0$ there must be a $\phi_c(k) \in R$, so that

$$\Delta y(k+1) = \phi_c(k)\Delta u(k) \tag{10}$$

where $\Delta y(k+1) = y(k+1) - y(k)$; $\Delta u(k) = u(k) - u(k\text{-}1)$.

In order to avoid producing too large control signal and steady-state error, the criterion function of the control input is expressed as follow:

$$J(u(k)) = \left|y^*(k+1) - y(k)\right|^2 + \lambda\left|u(k) - u(k-1)\right|^2 \tag{11}$$

where λ>0 is a weight factor; $y^*(k+1)$ is the desired output at $t = k+1$.

For reducing the sensitivity of the parameter estimation to the external interference, the criterion function of estimating Pseudo-partial derivative is proposed as:

$$J(\phi_c(k)) = \left|y(k) - y(k-1) - \phi_c(k)\Delta u(k-1)\right|^2 + \mu\left|\phi_c(k) - \hat{\phi}_c(k-1)\right|^2 \tag{12}$$

where μ >0 is a weight factor; $\hat{\phi}_c(k)$ is the estimated value of $\phi_c(k)$. Hence, the corresponding MFAC algorithms can be described as follows:

$$\hat{\phi}_c(k) = \hat{\phi}_c(k-1) + \frac{\eta\Delta u(k-1)}{\mu + \Delta u(k-1)^2}(\Delta y(k) - \hat{\phi}_c(k-1)\Delta u(k-1)) \tag{13}$$

$$u(k) = u(k-1) + \frac{\rho\hat{\phi}_c(k)}{\lambda + \left|\hat{\phi}_c(k)\right|^2}(y^*(k+1) - y(k)) \tag{14}$$

where $\lambda > 0, \mu > 0, \rho \in (0,1]$ and $\eta \in (0,1]$.

3.2 PSA-MFAC law design

From Eqs. (13) and (14), the control parameters λ, μ , ρ and η need to be adjusted. Weight factor λ is used to restrain the value of the control input. The function of ρ is used to adjust the response speed of MFAC. Weight factor μ is used to restrain the estimated value of $\phi_c(k)$. The function of η is used to adjust the estimated speed of $\phi_c(k)$. ρ and λ have greater effects on controller performance than μ and η during the operation of MFAC. If ρ is too large, the control system will be overshoot, otherwise its response speed will be slow. If λ is too large, it is easy to cause the control system to delay, otherwise the system will diverge easily. In order not to introduce additional control parameters, based on the gradient descent method, the control parameters of MFAC can be estimated by considering the estimation error of system and above characteristics of parameters. And the estimation algorithm can be expressed as follow:

$$ve(k+1) = ve(k) - \left|\frac{(er(k) - er(k-1))}{h} \times er(k)\right| \tag{15}$$

$$\eta(k+1) = \eta(k) - \left|\frac{(er(k) - er(k-1))}{h} \times er(k)\right| \tag{16}$$

$$\mu(k+1) = \mu(k) - ve(k) \times er(k) \tag{17}$$

$$\rho(k+1) = \rho(k) + \left|\frac{(er(k) - er(k-1))}{h} \times er(k)\right| \tag{18}$$

$$\lambda(k+1) = \lambda(k) + ve(k+1) \times er(k) \tag{19}$$

where h is step-size; η, ρ and $ve \in (0,1]$; μ and λ >0. By substituting Eqs. (15)-(19) to Eqs. (13) and (14), the control law can eventually be described as:

$$\hat{\phi}_c(k) = \hat{\phi}_c(k-1) + \frac{(\eta(k-1) - \left|K \times er(k-1)\right|)\Delta u(k-1)}{\mu(k-1) - (ve(k-1) - \left|K \times er(k-1)\right|)er(k-1) + \Delta u(k-1)^2} (\Delta y(k) - \hat{\phi}_c(k-1)\Delta u(k-1)) \tag{20}$$

$$u(k) = u(k-1) + \frac{(\rho(k-1) + \left|K \times er(k-1)\right|)\hat{\phi}_c(k)}{\lambda(k-1) + (ve(k-1) - \left|K \times er(k-1)\right|)er(k-1) + \left|\hat{\phi}_c(k)\right|^2} er(k) \tag{21}$$

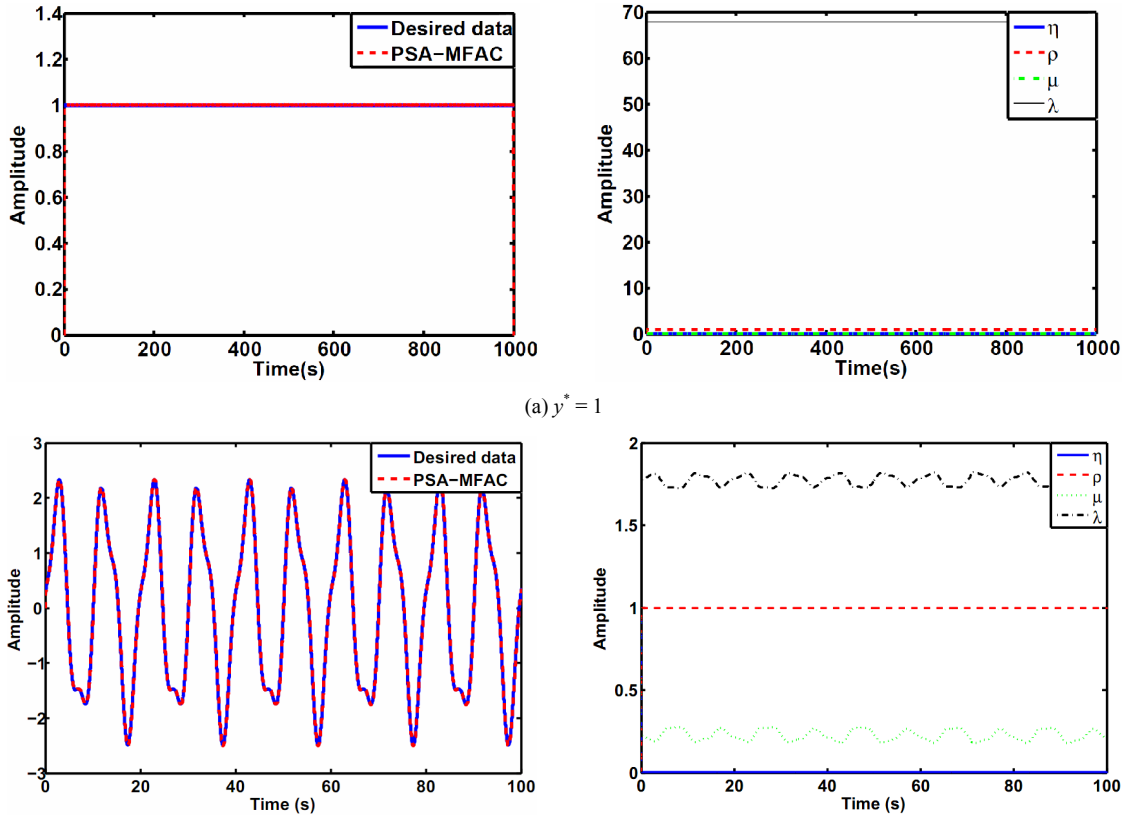

(a) $y^* = 1$

(b) $y^* = 0.5\cos(\pi/2t+\pi/3)+2\sin(\pi/5t)$

Fig. 3. Second-order system: $133/(s^2+25s)$.

where $K = (er(k)- er(k-1))/h$.

3.3 PSA-MFAC adaptability simulation

When initial values of PSA-MFAC parameters are constant, the simulation analysis of the adaptability can be conducted by changing controlled objects or tracking trajectory.

In this section, a second-order system $133/(s^2+25s)$, a third-order system $(-48s^2+550s+34328)/ (s^3+135s^2+33913s+321)$ and a nonlinear system $(y(i) = 0.00002u(i-2)+1.855u(i-1)^3-0.035u(i-3)u(i-1)^2)$ are selected as control objects for studying on the adaptability of PSA-MFAC. The second-order system has been set as control objects in Ref. [23], and the third-order system is the model of Ionic polymer metal composite (IPMC) made in our laboratory in Ref. [24]. A track square wave signal $y^* = 1$ and a trigonometric function signal $y^* = 0.5\cos(\pi t/2+\pi/3)+2\sin(\pi t /5)$ are applied as the reference signals. All signals are dimensionless. Based on the ranges of the control parameters, the initial values can be set as $\eta_0 = 1$, $\mu_0 = 1$, $\rho_0 = 0.1$, $\lambda_0 = 0.1$ and $ve_0 = 1$, respectively, and kept unchanged for all control objects. The step size is 0.001 s. The simulation results are shown in Figs. 3-5, and the key indicators of the dynamic performance are also reported in Tables 3 and 4.

Because of the unit step response characteristics of the second-order system and the third-order system (see Fig. 6), there are obvious difference between the dynamic performances of the second-order system and the third-order system as Table 3. From Figs. 3-5, and Tables 3 and 4, all the systems have better dynamic performance than without PSA-MFAC controller. The step response of second-order system is convergent, and the rising time of third-order system is shorten obviously, so the objective system can be guaranteed good response speed and tracking accuracy via the PSA-MFAC which doesn't need to adjust the control parameters repeatedly for different control objects or reference signals. Thus, the control scheme avoids cumbersome parameters adjusting process and has good adaptability and control accuracy.

4. Experimental study

4.1 Experimental system

The schematic diagram of the experimental measurement system is shown as Fig. 7. It consists of three PAMs, an angle sensor (CJMCU-99) which can measure rotation angles about all three axes, six 2-way solenoid valves (Shadow SPCU-S-1) and an Arduino UNO board. Three shadow 30 mm air muscles are used as actuators for bionic elbow joint. Every muscle can produce forces up to 700 N at pressures of only less than 3.5 bar, and its contraction can reach to 35 %. The measuring

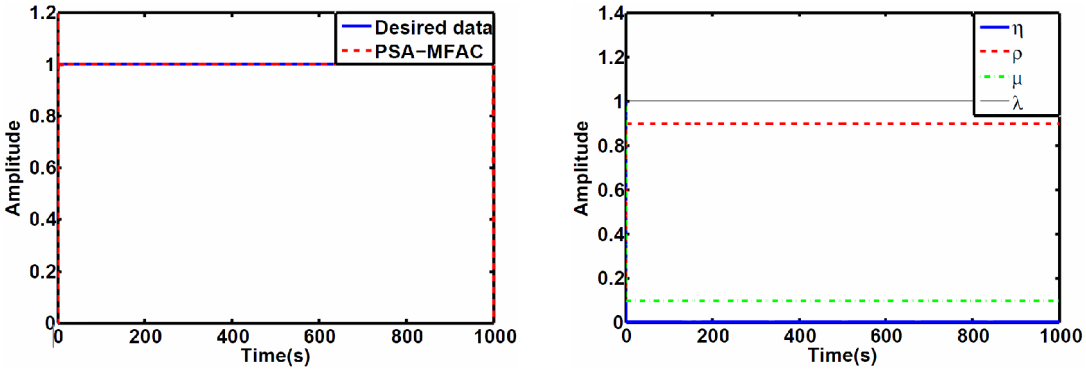

(a) $y^* = 1$

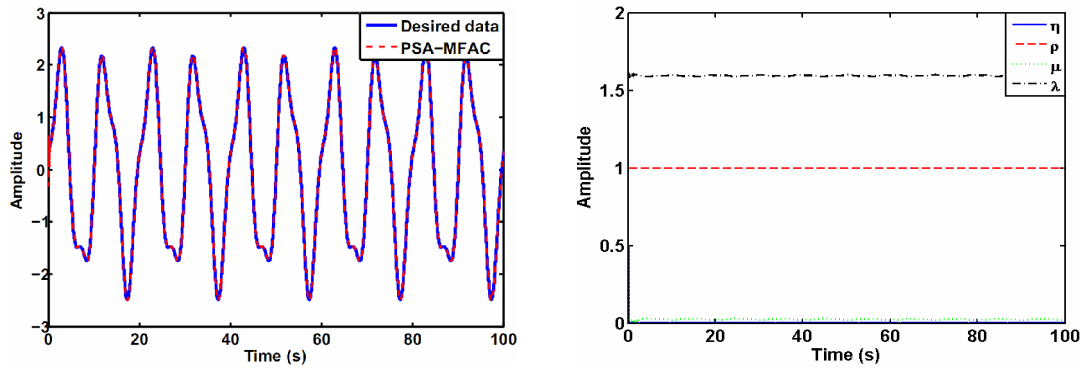

(b) $y^* = 0.5\cos(\pi/2t+\pi/3)+2\sin(\pi/5t)$

Fig. 4. Third-order system: $(-48s^2+550s+34328)/(s^3+135s^2+33913s+321)$.

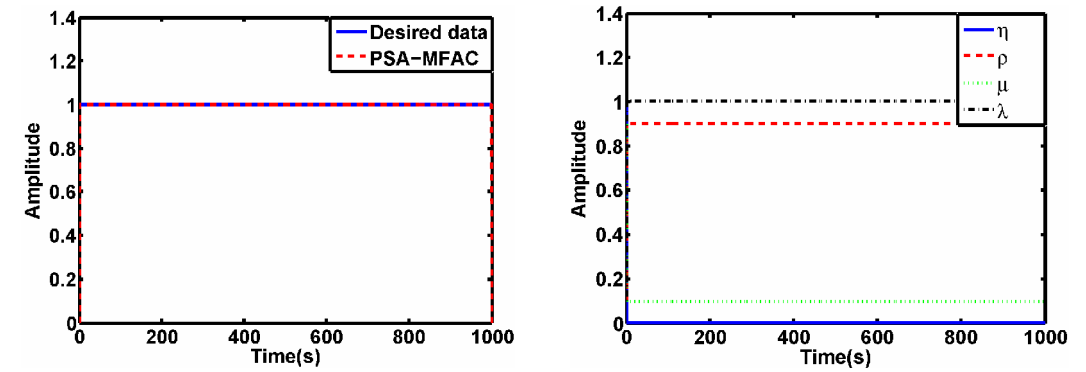

(a) $y^* = 1$

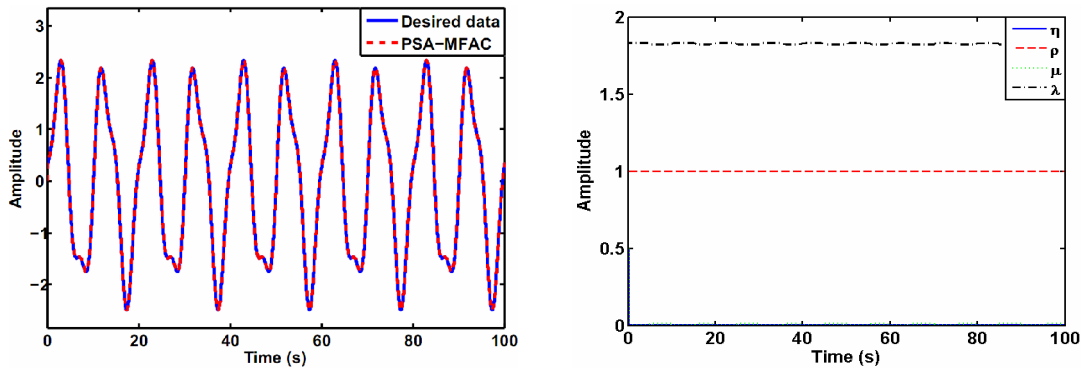

(b) $y^* = 0.5\cos(\pi/2t+\pi/3)+2\sin(\pi/5t)$

Fig. 5. Nonlinear system: $(y(i) = 0.00002u(i-2)+1.855u(i-1)^3-0.035\ u(i-3)u(i-1)^2)$.

range of the angle sensor is 0~360º. The sensor data is collected and sent to the PC via the Arduino UNO board. The PC contains an inverse kinematic model, three PSA-MFAC controllers and three PWM generators. Based on the data $\boldsymbol{\theta}$ (ψ, θ, φ), desired angles $\boldsymbol{\theta}_d$ (ψ_d,θ_d, φ_d) and the inverse kinematic model, the lengths of PAMs $\mathbf{L}(l_1, l_2, l_3)$ and the desired lengths of PAMs $\mathbf{L_d}(l_{d1}, l_{d2}, l_{d3})$ can be obtainted. Each PAM has a PSA-MFAC controller and a PWM generator. Based on the **error** = $\mathbf{L_d}$-$\mathbf{L}$, the three PAMs can be controlled respectively via three PSA-MFAC controllers and three PWM generators, which results in the rotation angles could be controlled. The schematic diagram of PSA-MFAC is shown in Fig. 8, and the experimental measurement system is constructed as Fig. 9.

4.2 Results and discussion

In this experiment, the bionic elbow joint is unloaded, and the pressure of the PAMs' air inlet end is maintained at 2 bar. The carrier wave is 5sawtooth (350πt) +5. The bionic elbow joint is controlled by PID, MFAC and PSA-MFAC controllers, respectively. The control parameters of the PID controller are set as k_p = 1, k_i = 0.01 and k_d = 0, respectively. The control parameters of the MFAC controller are set as η = 0.8, μ = 0.01, ρ = 0.001 and λ = 0.001, respectively. The initial values of PSA-MFAC's control parameters can be set as η_0 = 1, μ_0 = 1, ρ_0 = 0.1, λ_0 = 0.1 and ve_0 = 1, respectively. Based on the con-

Table 3. Indicators of dynamic performance (y^* = 1).

Control object	Rising time (s)	Overshoot (%)	Settling time(s)	Steady state error
Second-order system	2.42	0	2.42	3.33e-16
Third-order system	0.024	20	8	0
Nonlinear system	0.007	0.14	0.017	0

Table 4. Indicators of dynamic performance (y^* = 0.5cos (πt/20+π/3) +2sin (πt /50)).

Control object	Second-order system	Third-order system	Nonlinear system
Tracking accuracy (%)	0.22	0.14	0.08

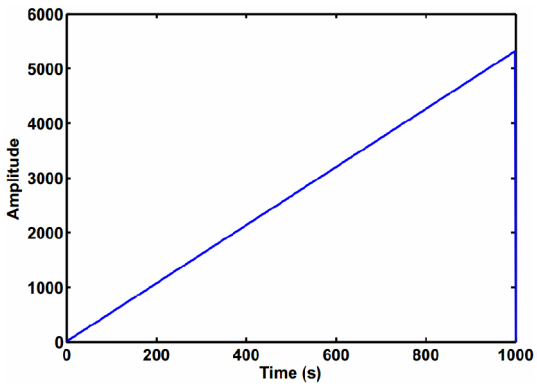

(a) Second-order system

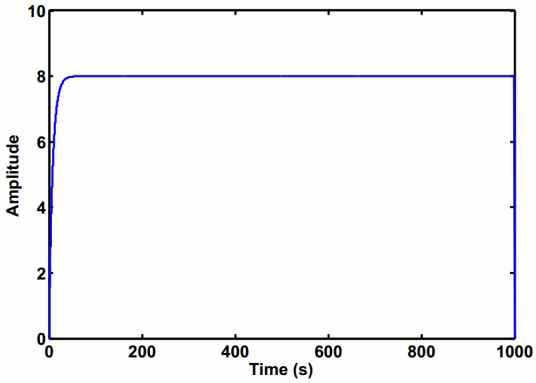

(b) Third-order system

Fig. 6. The unit step responses.

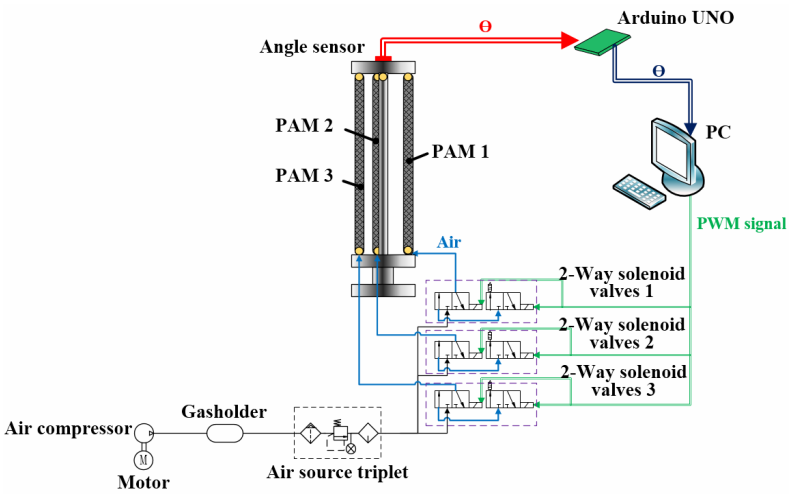

Fig. 7. Schematic diagram of the experimental measurement system.

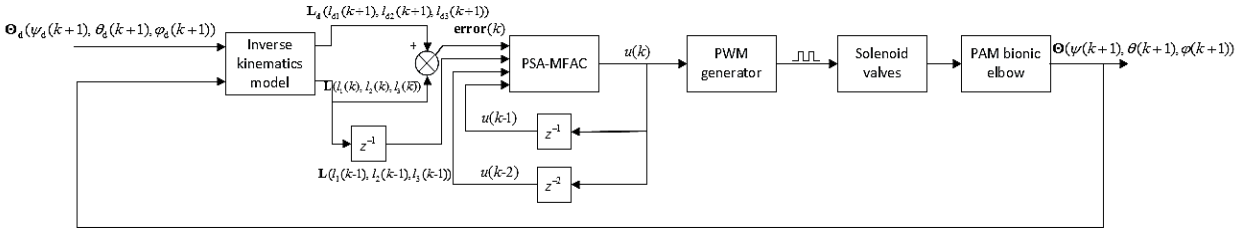

Fig. 8. Control schematic diagram.

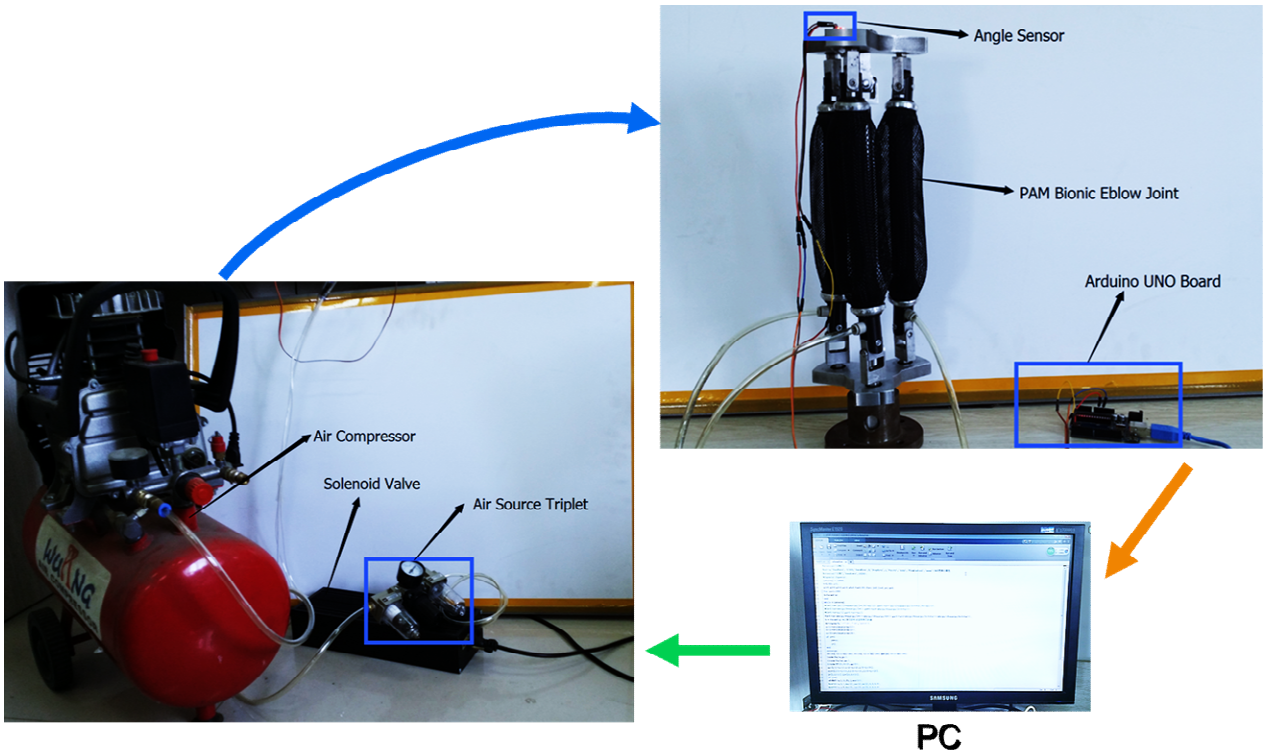

Fig. 9. Experimental measurement system.

trol requirements, the range of the allowable error is set [-0.4°, 0.4°]. The functions $\theta_d = \pi/12$, θ_d = abs (π/6sin (π/2t)) and θ_d = π/12square(π/2t, 50)+π/12 are applied as the reference signals. The experiment results are shown in Figs. 10-12.

In this paper, the rotation angle error equals to the difference between the desired angle and the measurement angle obtained via CJMCU-99. Moreover, all control experiments were all under same environmental conditions, and we used kalman filter algorithm to reduce the influence of magnetic interference. Then the analysis of the experiment results are as follows:

(1) In Fig. 10, the PID controller's overshoot is 9.7 %, settling time is about 0.35 s, and steady state error is about 0.008 rad (0.45°) beyond the range of the allowable error. Thus, the posture of the movement platform is adjusted again, which leads to a dithering phenomenon at 0.6 s to 1.3 s. The final steady state error of PID controller is about 0.003 rad (0.17°). The MFAC controller's overshoot is 10.3 %, settling time is about 0.2 s, and steady state error is about 0.002 rad (0.11°). The PSA-MFAC controller's overshoot is 8 .8 %, settling time is about 0.2 s, and steady state error is about 0.002 rad (0.11°). Thus, the PSA-MFAC controller has a better dynamic performance than the other controllers.

(2) Compared with the other controllers, the PID controller fails in compensating for the nonlinearity of PAM, so it has the worst dynamic performance as shown in Fig. 11. The tracking accuracy of the PID controller is 15 %. Because the control parameters are constant, the control input of the MFAC controller is so large that a dithering phenomenon is appeared when the reference signal is close to the wave peak. The tracking accuracy of the MFAC controller is 9.5 %. The PSA-MFAC controller not only overcomes the nonlinearity of PAM but also has a better smoothness than the other controllers in the trajectory tracking. The tracking accuracy of the PSA-MFAC controller is 3.8 %.

(3) In Fig. 12, the PID controller's overshoot is 5.7 %, set-

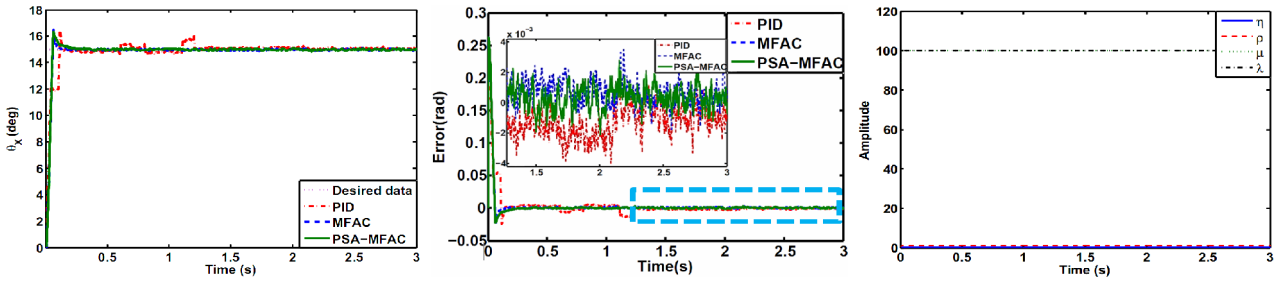

(a) Trajectory tracking (b) Trajectory error (c) Control parameters of PSA-MFAC for PAM1

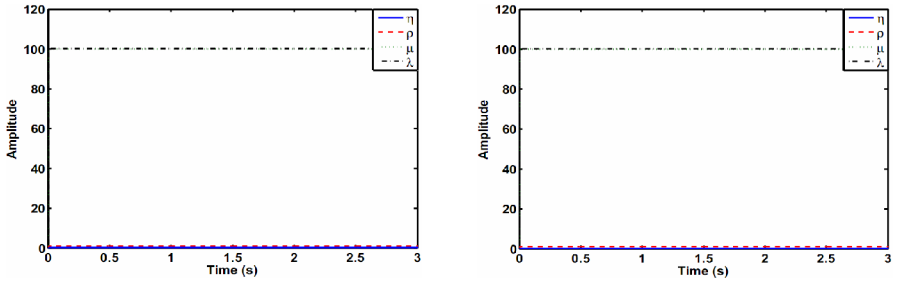

(d) Control parameters of PSA-MFAC for PAM2 (e) Control parameters of PSA-MFAC for PAM3

Fig. 10. Trajectory tracking ($\theta_d = \pi/12$).

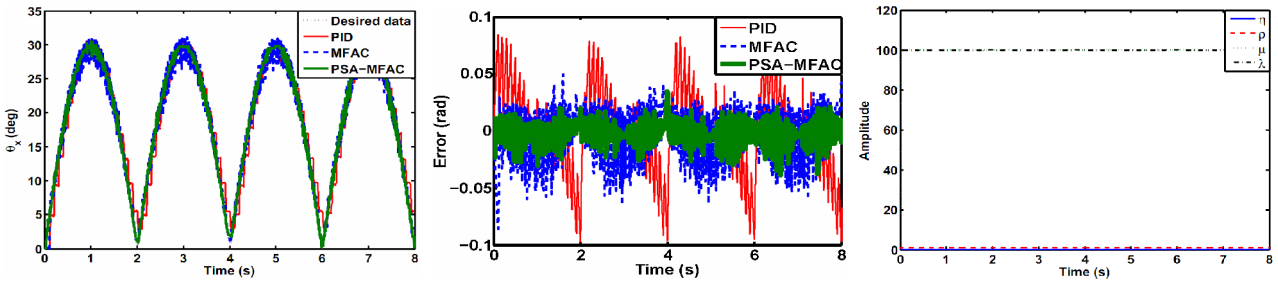

(a) Trajectory tracking (b) Trajectory error (c) Control parameters of PSA-MFAC for PAM1

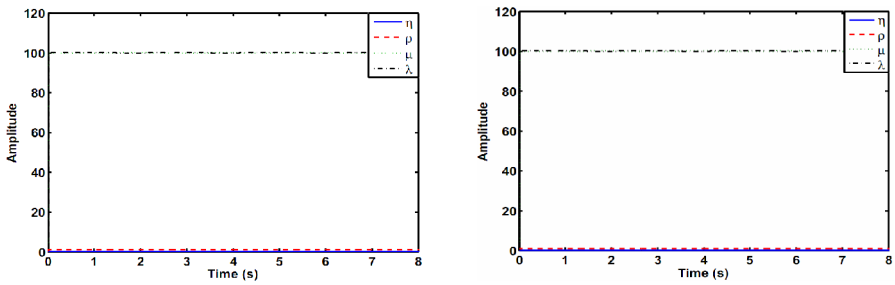

(d) Control parameters of PSA-MFAC for PAM2 (e) Control parameters of PSA-MFAC for PAM3

Fig. 11. Trajectory tracking ($\theta_d = \text{abs}(\pi/6\sin(\pi/6\sin(\pi t/2)))$).

tling time is about 0.35 s, and steady state error is about 0.005 rad (0.29°). However, there is a dithering phenomenon in the second cycle because of the nonlinearity of PAM. The MFAC controller's overshoot is 5.5 %, settling time is about 0.25 s, and steady state error is about 0.007 rad (0.4°). The PSA-MFAC controller's overshoot is 1 %, settling time is about 0.22 s, and steady state error is about 0.003 rad (0.17°). It is observed that PSA-MFAC has a better dynamic performance than the other controllers.

5. Conclusion

In this article, a novel PAM bionic elbow joint was designed and its inverse kinematic model was also established. Based on the MFAC theory and the gradient descent method, a PSA-MFAC scheme was presented by considering the estimation error of system and characteristics of the control parameters, and then its adaptability simulation was carried out. From the results, the PSA-MFAC controller has a good adapt-

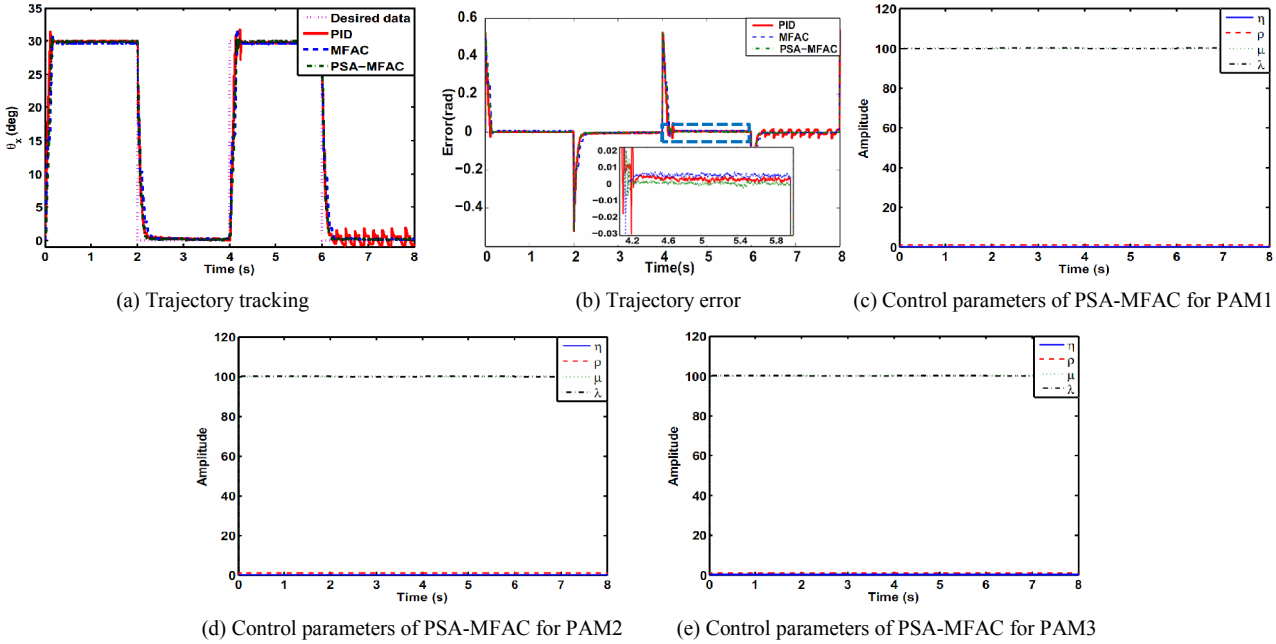

(a) Trajectory tracking (b) Trajectory error (c) Control parameters of PSA-MFAC for PAM1

(d) Control parameters of PSA-MFAC for PAM2 (e) Control parameters of PSA-MFAC for PAM3

Fig. 12. Trajectory tracking (θ_d = π/12square(πt/2, 50)+π/12).

ability. Then, based on the inverse kinematic model, a PID controller, a MFAC controller and a PSA-MFAC controller were applied to the PAM bionic elbow joint, and then motion control experiments were conducted. As the experiment results shown, the PSA-MFAC controller has better dynamic performance, smoothness and tracking accuracy than the other controllers.

Acknowledgment

This work was supported by the National High Technology Research and Development Program of China (863 program) under Grant No. 2015AA042302, and the Equipment Pre-Research Program of China under Grant No. 62501040412.

References

[1] H. A. Baldwin, Realizable models of muscle function, *Proceedings of the First Rock Biomechanics Symposium*, New York (1969) 139-148.

[2] D. G. Caldwell, A. Razak and M. J. Goodwin, Braided pneumatic muscle actuators, proceedings of the IFAC conference on intelligent autonomous vehicles, *Southampton* (1993) 507-512.

[3] Y.-L. Park, B. Chen, N. O. Pérez-Arancibia, D. Young, L. Stirling, R. J. Wood, E. C. Goldfield and R. Nagpal, Design and control of a bio-inspired soft wearable robotic device for ankle-foot rehabilitation, *Bioinspiration & Biomimetics*, 9 (2014) 1-17.

[4] Sawicki and Ferris, A pneumatically powered knee-ankle-foot orthosis (KAFO) with myoelectric activation and inhibition, *Journal of NeuroEngineering and Rehabilitation*, 6 (23) (2009) 1-16.

[5] E. T. Roche, R. Wohlfarth, J. T. B. Overvelde, N. V. Vasilyev, F. A. Pigula, D. J. Mooney, K. Bertoldi and C. J. Walsh, Actuators: A bioinspired soft actuated material, *Advanced Materials*, 26 (8) (2014) 1145.

[6] K. Junius, P. Cherelle, B. Brackx, J. Geeroms, T. Schepers, B. Vanderborght and D. Lefeber, On the use of adaptable compliant actuators in prosthetics, rehabilitation and assistive robotics, *Robot Motion and Control* (2013).

[7] J. Wang, Y. Jin and Z. Tang, Mechanism design and realization of joint of pneumatic muscle of manipulator, *Machine-tool & Hydraulics*, 37 (7) (2009) 86-92 (in Chinese).

[8] G. Andrikopoulos, G. Nikolakopoulos, I. Arvanitakis and S. Manesis, Switching model predictive control of a pneumatic artificial muscle, *International Journal of Control, Automation, and Systems*, 11 (6) (2013) 1223-1231.

[9] V. T. Jouppila, S. A. Gadsden, G. M. Bone, A. U. Ellman and S. R. Habibi, Sliding mode control of a pneumatic muscle actuator system with a pwm strategy, *International Journal of Fluid Power*, 15 (1) (2014) 19-31.

[10] R. M. Robinson, C. S. Kothera and N. M. Wereley, Control of a heavy-lift robotic manipulator with pneumatic artificial muscles, *Actuators*, 3 (2014) 41- 65.

[11] B.-S. Kang, Compliance characteristic and force control of antagonistic actuation by pneumatic artificial muscles, *Meccanica*, 49 (2014) 565-574.

[12] X. Zhu, G. Tao, B. Yao and J. Cao, Adaptive robust posture control of a parallel manipulator driven by pneumatic muscles, *Automatica*, 44 (2008) 2248-2257.

[13] L.-W. Lee and I.-H. Li, Design and implementation of a robust FNN-based adaptive sliding-mode controller for pneumatic actuator systems, *Journal of Mechanical Science*

and Technology, 30 (1) (2016) 381-396.
[14] L. Liu, J. Li, Y. Liu, J. Leng, J. Zhao and J. Zhao, Electric field induced variation of temperature and entropy in dielectric elastomers, *Journal of Mechanical Science and Technology*, 29 (1) (2015) 109-114.
[15] B. Tondu, Robust and accurate closed-loop control of mckibben artificial muscle contraction with a linear single integral action, *Actuators*, 3 (2014) 142-161.
[16] X. Chang and J. H. Lilly, Fuzzy control for pneumatic muscle tracking via evolutionary tuning, *Intelligent Automation & Soft Computing*, 9 (4) (2013) 227-244.
[17] H. P. H. Anh and K. K. Ahn, Hybrid control of a pneumatic artificial muscle(PAM) robot arm using an inverse NARX fuzzy model, *Engineering Applications of Artificial Intelligence*, 24 (2010) 697-716.
[18] Y. Zhu and Z. Hou, Data-driven MFAC for a class of discrete-time nonlinear systems with RBFNN, *IEEE Transactions on Neural Networks and Learning Systems*, 25 (5) (2014) 1013-1020.
[19] L. dos S. Coelho and A. A. R. Coelho, Model-free adaptive control optimization using a chaotic particle swarm approach, *Chaos, Solitons and Fractals*, 41 (2009) 2001-2009.
[20] L. Yu, W. Tao, A. Wei and W. Yu, Model-free adaptive control for the ball-joint robot driven by PMA group, *Robot*, 35 (2) (2013) 129-134 (in Chinese).
[21] Y. Gang, L. Baoren and F. Xiaoyun, Parallel manipulator driven by pneumatic muscle actuators, *Chinese Journal of Mechanical Engineering*, 42 (7) (2006) 39-45 (in Chinese).
[22] L. D. S. Coelho and A. A. R. Coelho, Model-free adaptive control optimization using a chaotic particle swarm approach, *Chaos, Solitons & Fractals*, 41 (4) (2009) 2001-2009.
[23] K. K. Tan and T. H. Lee, S. N. Huang, Adaptive- predictive control of a class of SISO nonlinear systems, *Dynamics and Control*, 11 (2) (2001) 151-174.
[24] B. Zhang and W. D. Zhang, Adaptive predictive functional control of a class of nonlinear systems, *ISA Transactions*, 45 (2) (2006) 175-183.
[25] G. Feng, A compensating scheme for robot tracking based on neural networks, *Robotics and Autonomous Systems*, 15 (1995) 100-206.
[26] L. Hao, Y. Chen and Z. Sun, The sliding mode control for different shapes and dimensions of IPMC on resisting its creep characteristics, *Smart Materials and Structure*, 24 (2015) 045040.

Hui Yang was born in Jinzhou, China, in 1987. He received the B.S. degree and M.S. degree in machinery design and manufacture from Liaoning Shihua University, Fushun, China in 2010 and 2013, respectively. He is currently a Ph.D. candidate at the Northeastern University, Shenyang, China. His research interests include modeling and control of PAM and compliance control of the bionic manipulator actuated by artificial muscles. He is a student member of IEEE and International Society of Bionic Engineering.

Lina Hao was born in Zhuanghe, China, in 1968. She received the B.S. degree in machinery design and manufacture from Shenyang Ligong University, Shenyang, China in 1989, M.S. degree in solid mechanics and Ph.D. degree in control theory and control engineering from Northeastern University, Shenyang, China in 1994 and 2001, respectively. Currently, she is a Professor in Department of Mechanical Engineering and Automation in Northeastern University, China. Her research interests include robot system and intelligent control, intelligent structure and precision motion control system, pattern recognition and condition monitoring. Prof. Hao is selected as a hundred-level member in "Pacesetter Project" Liaoning province, China, a member of International Society of Bionic Engineering and a member of Chinese Association of Automation System Simulation Discipline and Robot Discipline Committee.